INTERNATIONAL JOURNAL OF CLIMATOLOGY
Int. J. Climatol. **24**: 841–852 (2004)
Published online 14 May 2004 in Wiley InterScience (www.interscience.wiley.com). DOI: 10.1002/joc.1040

RE-EVALUATING ANTARCTIC SEA-ICE VARIABILITY AND ITS TELECONNECTIONS IN A GISS GLOBAL CLIMATE MODEL WITH IMPROVED SEA ICE AND OCEAN PROCESSES

JIPING LIU,[a,b]* XIAOJUN YUAN,[c] DOUGLAS G. MARTINSON[b,c] and DAVID RIND[a,b]
[a] *NASA Goddard Institute for Space Studies, New York, NY 10025, USA*
[b] *Department of Earth and Environmental Sciences, Columbia University, Palisades, NY 10964, USA*
[c] *Lamont–Doherty Earth Observatory of Columbia University, Palisades, NY 10964, USA*

Received 10 August 2003
Revised 24 February 2004
Accepted 24 February 2004

ABSTRACT

This study re-evaluated simulated Antarctic sea-ice variability and its teleconnections in a NASA Goddard Institute for Space Studies (GISS) coupled global climate model (CGCM) with improved sea-ice and ocean processes. With the improvements to the parameterizations of sea-ice dynamics and thermodynamics and of sub-grid-scale ocean processes, the new version of the GISS/CGCM does indeed do a better job in the representations of the local/regional ice–ocean interactions with regard to (1) the seasonal distributions of the Antarctic sea-ice edges (SIE), and (2) the vertical temperature and salinity structure in the upper Southern Ocean and surface air temperature (SAT) climatology in the southern high latitudes compared with the control version. However, these encouraging local/regional improvements do not extend to the simulations of the polar and extrapolar climate teleconnections. There is no obvious change to the simulations of the dominant spatial covarying patterns of the SAT variability on either the regional (southern high latitudes) or global scales. The simulated teleconnections between Antarctic SIE and global SAT still show the weak El Niño–southern oscillation like correlation pattern in the eastern tropical Pacific, though the new version generates a stronger tropical Indian component. Some dominant observed teleconnection patterns in the western extreme of the tropical Pacific and over the tropical continents (in-phase relationship between tropical South America and Africa) are still not well represented or are missed in the Antarctic SIE and global SAT lead/lag correlation maps and the empirical orthogonal function analysis on those correlation maps. The possible causes of the weak teleconnections in the improved GISS/CGCM are briefly discussed. Copyright © 2004 Royal Meteorological Society.

KEY WORDS: Antarctic sea-ice variability; coupled global climate model; improved GISS/CGCM; teleconnections

1. INTRODUCTION

Coupled global climate models (CGCMs) represent powerful tools for understanding interactions among the atmosphere, sea ice and ocean system and for making quantitative projections of future climate change resulting from natural variability and anthropogenic effects. However, the largest disagreements among CGCMs' simulations of present climate are in the polar regions (e.g. Houghton *et al*., 2001). Model projections of greenhouse-gas-induced global warming indicate enhanced climate sensitivity at high latitudes largely due to the positive ice–albedo feedback (e.g. Mitchell *et al*., 1995; Rind *et al*., 1995; Houghton *et al*., 2001).

The signatures of climate teleconnections involved in the Antarctic have been revealed in many studies (e.g. Yuan and Martinson, 2000; see Carleton (2003) for a review). For example, the El Niño–southern oscillation (ENSO) variability pattern shows an Antarctic dipole structure (Yuan and Martinson, 2000), which is characterized by opposing anomalies in the surface temperature and sea ice between the Ross/Amundsen

* Correspondence to: Jiping Liu, School of Earth and Atmospheric Sciences, Georgia Institute of Technology, 311 Ferst Drive, Atlanta, GA 30332–0340, USA; e-mail: jliu@eas.gatech.edu

Sea sector and eastern Bellingshausen/Weddell Gyre sector of the Southern Ocean. However, it remains undetermined as to whether current CGCMs have the capability to reproduce the polar–extrapolar covarying climate patterns that are observed in nature. Concerns include the facts that: (1) the largest disagreements among CGCMs reflect the weakness of our understanding of the complicated atmosphere–sea-ice–ocean interactions and the sensitivity of polar climate to different formulations of various physical processes; and (2) the enhanced climate sensitivity might be an artifact of the crude treatment of sea-ice processes in CGCMs.

To address these concerns in a systematic way, we first investigated three state-of-the-art CGCMs (GISS: Goddard Institute for Space Studies; NCAR: National Center for Atmospheric Research; and GFDL: Geophysical Fluid Dynamics Laboratory) for their capability to simulate Antarctic sea-ice variability and its climate–relevant influences by evaluating the extent to which the models can capture observed polar–extraploar covarying climate structure as identified in Yuan and Martinson (2000). The results show that, despite some encouraging agreements between simulated Antarctic sea-ice variability and its global teleconnections relative to that documented in the observations, the models still differ from observations in some noteworthy ways (see Liu *et al*. (2002) for details). Second, we have then incorporated more realistic sea-ice dynamics and thermodynamics and sub-grid-scale ocean physical parameterizations in the GISS/CGCM to represent sea-ice conditions and atmosphere–sea-ice–ocean interactions more accurately (Liu *et al*., 2003a,b), attempting to result in proper polar–extrapolar covariability.

The purpose of this paper is to reassess whether or not the GISS/CGCM with improved sea-ice and ocean parameterizations (hereafter referred to as GISS_new) has a better ability to represent the observed Antarctic sea-ice variability and, as a result, polar–extrapolar climate teleconnection patterns than the control version (hereafter referred to as GISS_control) analysed in Liu *et al*. (2002). The GISS_new run combines (a) the viscous–plastic dynamic ice rheology (Zhang and Hibler, 1997; Zhang and Rothrock, 2000), (b) the Gent and McWilliams mesoscale eddy isopycnal mixing scheme with Visbeck scaling mixing coefficients (Gent and McWilliams, 1990; Gent *et al*., 1995; Visbeck *et al*., 1997; Griffies *et al*., 1998), (c) the Wajsowicz (1993) viscosity diffusion, (d) the more sophisticated surface albedo scheme (Schramm *et al*., 1997), (e) the penetration of shortwave radiation through sea ice (Grenfell and Maykat, 1977; Ebert *et al*., 1995), (f) the effects of including a sea-ice salinity budget (Curry and Webster, 1999), and (g) the changes to the ice–ocean boundary flux formulation (McPhee and Maykut, 1987; Holland and Jenkins, 1999); see Liu *et al*. (2003a,b) for detailed discussion regarding the control version of the GISS/CGCM and its improvements.

2. DATA AND MODEL OUTPUTS

The observed datasets used here are: (1) the surface air temperature (SAT) from the National Centers for Environmental Prediction (NCEP)–NCAR reanalysis from 1977 to 1999, and (2) Antarctic sea-ice edges (SIE; calculated from sea-ice concentrations) and sea-ice drifts (Emery *et al*., personal communication, 2001) derived from the satellite SMMR/SSMI from 1979 to 1997. Following the same procedures as in Liu *et al*. (2002), monthly SAT of the GISS_new scenario run (observed greenhouse gases are used from 1950 to 1990, then the CO_2 increases 1% per year from 1990) was interpolated onto a 5° by 5° grid from 1977 to 1999. We then removed any trend present in the SAT anomalies at each grid point to generate SAT*. The averaged global SAT has risen 0.72 °C and 0.77 °C during the above time period in the GISS_control and GISS_new runs respectively. Antarctic sea-ice concentrations of the GISS_new run were interpolated onto a 0.25° (latitude) by 1° (longitude) grid. The Antarctic SIE is defined as the equatormost position of the 30% of sea-ice concentration for each degree of longitude. The SIE was averaged into 12° longitude bands to generate 30 quasi-spatially independent time series around the globe. Monthly SIE anomalies for every 12° longitude band over the period 1979–97 were detrended to generate SIE*. To focus on interannual (and longer) variability, all time series were temporally smoothed by a Gaussian filter to remove variability with periods less than a year before generating detrended anomalies.

3. RESULTS

3.1. Climate model performance

Before evaluating whether or not the GISS_new run improves the simulations of observed connectivities between Antarctic SIE* and global SAT* compared with the GISS_control run, we first investigated whether (1) the observed Antarctic SIE distributions and (2) the dominant covarying spatial patterns in SAT* are better simulated in the GISS_new run. Based upon these analyses, we can obtain a preliminary understanding of similar/different performance between two runs.

The seasonal mean Antarctic SIE over the period 1979–97 is shown in Figure 1. Compared with the satellite observations, the GISS_new run does indeed improve the simulations of the Antarctic SIE distributions in

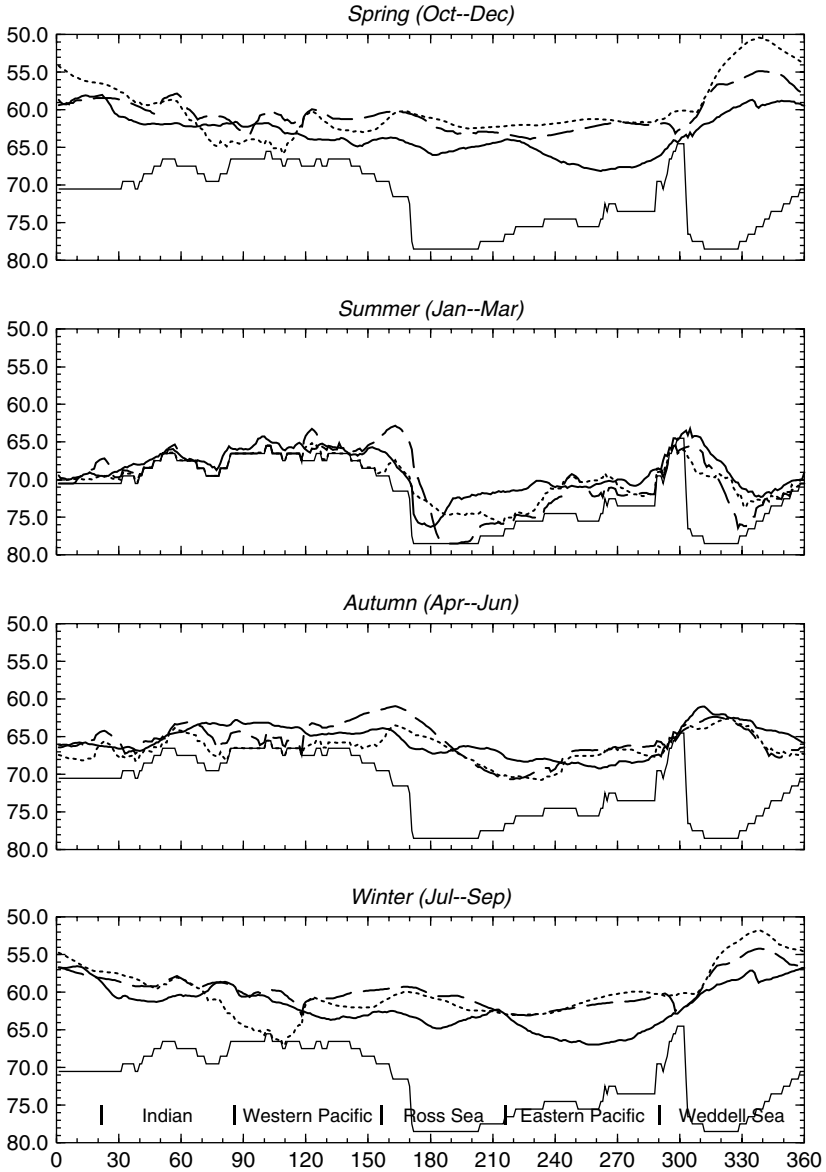

Figure 1. The seasonal mean Antarctic SIE (in degrees latitude). Solid line: SMMR/SSMI satellite observation; dotted line: GISS_control; dashed line: GISS_new; stair line: Antarctic continent

spring and winter. The spatial correlations in spring and winter between the observed and GISS_new SIE are 0.81 and 0.83 ($r^2 = 0.66$ and 0.68) respectively, versus 0.61 and 0.6 ($r^2 = 0.37$ and 0.36) in the GISS_control run. Thus, the GISS_new run describes almost twice as much of the observed SIE variance relative to the GISS_control run. Where are these improvements realized? In spring and winter, the SIE extends $\sim 8^\circ$ of latitude farther north in the GISS_control run than the observed SIE in the Weddell Sea. By contrast, the differences are reduced to $\sim 3-4^\circ$ latitude in the GISS_new run. Additionally, the GISS_new run eliminates extreme low sea-ice cover between the eastern Indian and the western Pacific sectors of the Antarctic present in the GISS_control run in spring and winter. However, sea-ice cover in the GISS_new run is still excessive in the eastern Pacific sectors of the Antarctic in spring and winter relative to the observations. In summer and autumn, by contrast, the GISS_new run does not yield improvements. In fact, the spatial correlations between the observed and GISS_new SIE are 0.81 and 0.61 respectively in summer and autumn, which are slightly poorer relative to the correlations between the observed and GISS_control SIE (0.85 and 0.64).

To determine why the GISS_new run produces a more realistic Antarctic SIE than the GISS_control run in the aforementioned regions during the cold seasons, we plotted the Antarctic sea-ice drifts in September (winter maximum sea-ice extent, Figure 2). In general, compared with the observations (Emery *et al.*, personal communication, 2001), the GISS_new run gives more reasonable ice drifts, whereas the ice drifts are too large in the GISS_control run (especially along the coastlines) due to the absence of shear stress. The GISS_new run also eliminates the excessive northward sea-ice advection in the Weddell Sea present in the GISS_control run, which is consistent with improved SIE simulations there. However, both runs show excessive northward

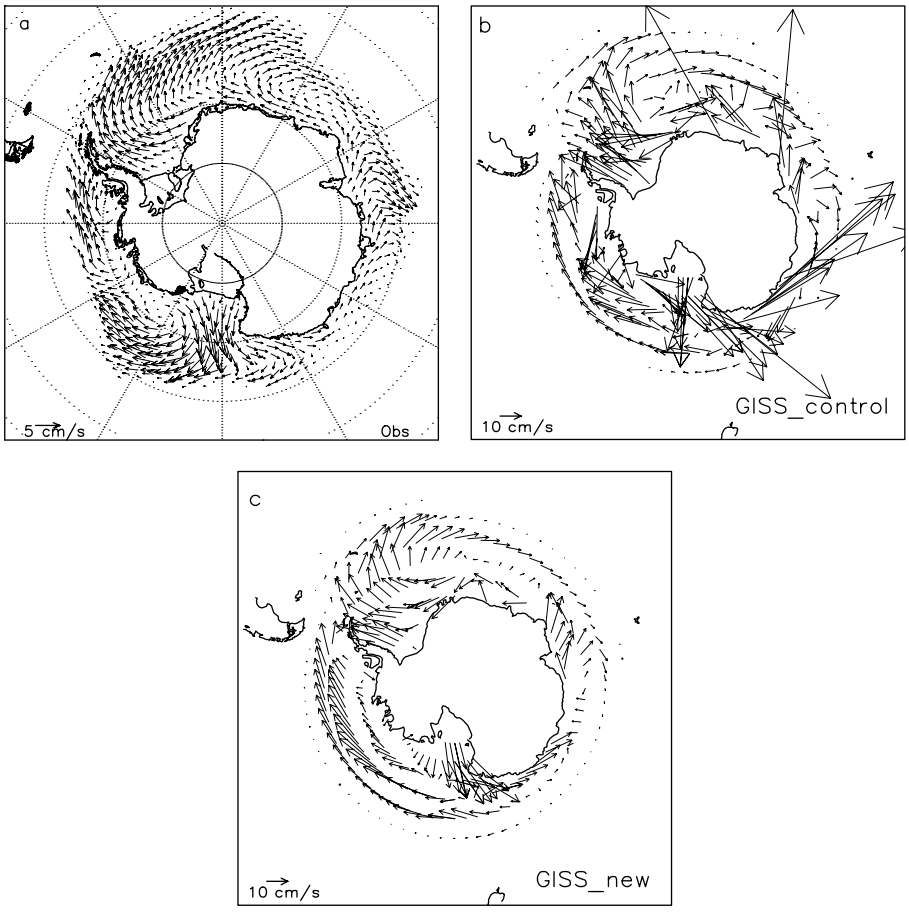

Figure 2. The (a) observed (derived from the satellite SSMR/SSMI) and simulated Antarctic sea-ice drifts (cm/s) in the (b) GISS_control and (c) GISS_new runs in September. Note the different scale vectors in the observations and model simulations

ice advection in the eastern Pacific, because the much weaker cyclonic atmospheric circulation there in both runs, compared with the NCEP–NCAR reanalysis (not shown), produces weaker northerly winds that limit northward ice advection. We then plotted the vertical ocean temperature and salinity profiles along 107.5 °E, 107.5 °W and 32.5 °W in September (Figure 3). Compared with the observations (Levitus and Boyer, 1994; Levitus *et al*., 1994), qualitatively speaking, the vertical temperature and salinity structures of the GISS_new run appear to be more realistic than the GISS_control run. For example, the GISS_new run leads to a warmer and saltier upper-ocean layer and more proper poleward spread of relatively warm deep water into the Weddell Sea (32.5 °W) relative to the GISS_control run, which approaches the observations (Levitus and Boyer, 1994; Levitus *et al*., 1994) and is consistent with improved SIE simulations in the Weddell Sea. However, the simulated upper-ocean layer in the GISS_new run is still colder and fresher than the observations (Levitus and Boyer, 1994; Levitus *et al*., 1994); this reduces the contribution of heat from the relatively warm deep water into the surface layer, leading to extensive winter sea ice there (Martinson, 1990). The situation is similar in the eastern Pacific sector of the Antarctic (107.5 °W). By contrast, the simulated temperature of the upper-ocean layer in the GISS_new run is colder than the GISS_control run along 107.5 °E, which is also more akin to the observations (Levitus and Boyer, 1994; Levitus *et al*., 1994) and encourages sea-ice growth. Therefore, the GISS_new run produces a more realistic SIE between the eastern Indian and western Pacific sectors of the Antarctic. The more realistic Antarctic SIE distributions and temperature and salinity structure in the upper Southern Ocean suggests that local/regional ice–ocean interactions are captured better.

Focusing first on the southern high latitudes (45–90 °S), the averaged SAT climatology is slightly improved in the GISS_new run. The seasonal SAT differences in the southern high latitudes between the observations and the GISS_new run (the GISS_control run) are −0.23 (0.14) °C, −0.06 (0.21) °C, 1.15 (1.65) °C, and 1.95 (3.00) °C in spring, summer, autumn, and winter respectively. An empirical orthogonal function (EOF) analysis was then applied to the observed and model-based SAT* in the southern high latitudes (not shown). The GISS_new run (like the GISS_control run) still shows an anomalous Antarctic-wide coherency extending to subpolar regions in the first mode, though the GISS_new run occupies 38.8% of the total variance, which is more realistic relative to the 43.6% in the GISS_control run compared with 24.8% in the observations. As for the second mode, both runs capture the Antarctic dipole (the strong out-of-phase relationship between the eastern Pacific and Atlantic sectors). However, the phase relationship between the Antarctic dipole and the Indian sector of the Antarctic is better simulated in the GISS_control run than the GISS_new run.

We also conducted an EOF analysis on the global SAT* (Figure 4). The GISS_new and GISS_control runs have quite similar dominant patterns: (1) Neither of them captures the main features in Figure 4(a1), especially the strong in-phase relationship between the tropical Indian and Atlantic. The observed SAT* variability in the tropical continents (tropical Africa and South America) is still underestimated in the GISS_new run. The GISS_new run produces a signal in the western tropical Pacific (Figure 4(c1)) that is not present in the GISS_control run (Figure 4(b1)). However, this signal is out of phase with southern polar regions in the GISS_new run, whereas they are in phase in the observations. (2) The tropical ENSO-like pattern in Figure 4(a2) shows up in both runs. Like the GISS_control run (Figure 4b2), the GISS_new run (Figure 4(c2)) does not produce the observed out-of-phase relationship between the eastern and western tropical Pacific in Figure 4(a2). (3) None of the runs (Figure 4(b3) and (c3)) captures the observed negative correlation between (a) the western extreme of the tropical and southern Pacific and (b) the eastern tropical Pacific and eastern Ross/Amundsen sector of the Southern Ocean in Figure 4(a3). As stated in Liu *et al*. (2002), the coarse resolution of the GISS/CGCM is not good enough to resolve the complex tropical ocean dynamics, leading to the poor atmospheric responses to the ENSO variability.

3.2. Polar–extrapolar teleconnections

Repeating the statistical analyses in Liu *et al*. (2002), the teleconnection patterns of the GISS_new run were identified by correlating 30 Antarctic SIE* time series with global SAT* at half-year lag intervals up to, leading and lagging 2 years. This generates a total of 270 global correlation maps.

Figure 5 is a collection of the correlation maps showing particular noteworthy correlation patterns (as discussed below) associated with the underlined SIE* regions at zero lag. Both the GISS_new and GISS_control

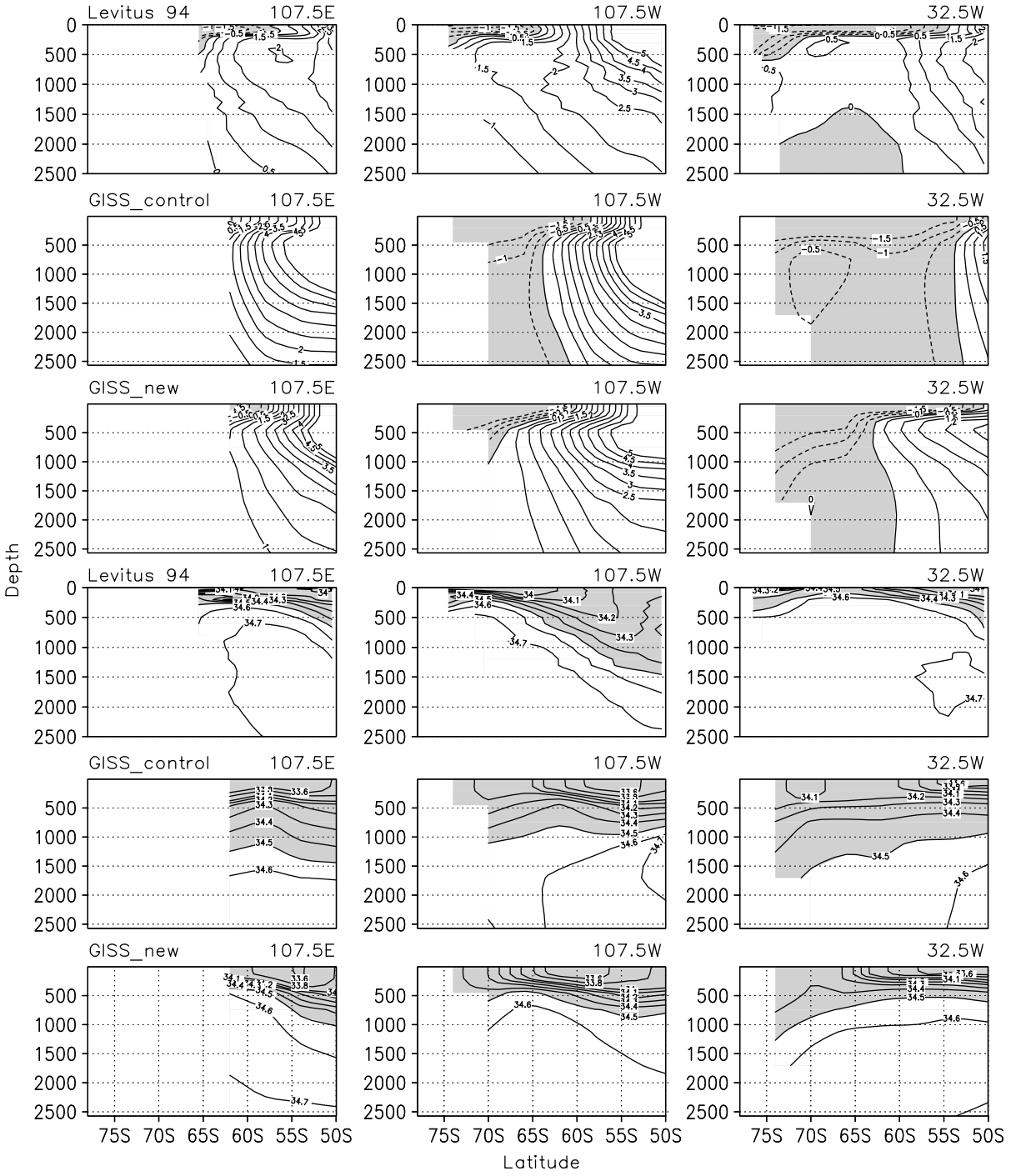

Figure 3. The vertical ocean temperature (upper three rows) and salinity (lower three rows) profiles along 107.5 °E, 107.5 °W and 32.5 °W in September from the observations (Levitus and Boyer, 1994; Levitus *et al.*, 1994), GISS_control and GISS_new runs (temperature below 0 °C and salinity below 34.5 ppt are shaded)

runs capture the tropical ENSO-like pattern (Figure 5(a1,a2)), the meridional banding structure in the Pacific (Figure 5(a3)), and the Antarctic dipole (Figure 5(a3)).

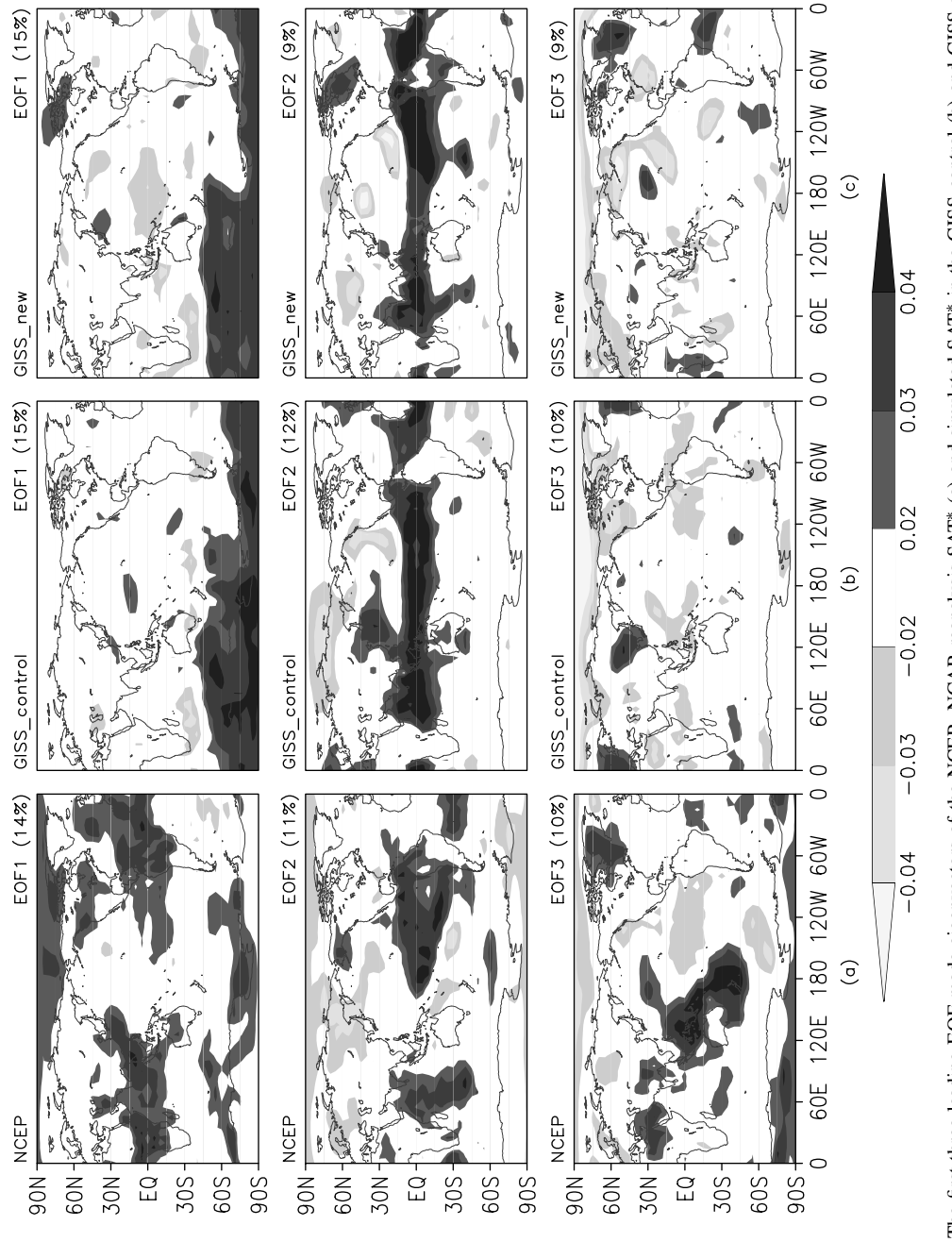

Figure 4. The first three leading EOF mode eigenvectors of the NCEP–NCAR reanalysis SAT* (a) and simulated SAT* in the GISS_control (b) and GISS_new (c) runs

Figure 5. The linear correlation between the NCEP–NCAR reanalysis SAT* and satellite SIE* (a) between the simulated SAT* and SIE* of the GISS_control (b) and GISS_new (c) runs at zero lag. Correlations are for SIE* in the underlined regions with global SAT*. Cross-correlations above the 95% confidence level are 0.44 and 0.43 in the GISS_control and GISS_new runs respectively

(1) In the GISS_new run, the SIE* regions strongly sensitive to the ENSO-like pattern are between eastern Atlantic and western Indian sectors of the Antarctic (the underlined region A), and the western and central Weddell Sea (the underlined region B). They are slightly different from the western Indian sector of the Antarctic and the Bellingshausen Sea in the GISS_control run. Interestingly, the observed SIE* regions with high sensitivity to the ENSO phenomena fall between the underlined regions of the two runs. Compared with the observations, the phase of the correlation between SIE* (and local SAT*) in the underlined region A and the tropical ENSO signal is positive in the observations and the GISS_control run, but negative in the GISS_new run (Figure 5(a1,b1,c1)). For the SIE* (and local SAT*) in the underlined region B (Figure 5(a2,b2,c2)), the opposite is the case. That is, in the observations and the GISS_new run they are out of phase, whereas in the GISS_control run they are in phase. As in the GISS_control run, the magnitude of the model-generated ENSO-like correlation pattern in the eastern tropical Pacific is weaker than found in the observations (given that the correlations in the eastern tropical Pacific show more shared variance r^2 in the observations than both runs). However, like the observations, the GISS_new run generates a strong Indian centre (Figure 5(c1)) that covaries with the eastern tropical Pacific, whereas the GISS_control run does not (Figure 5(b1)). It appears that the amplitude of the simulated Nino3 index (which is defined as the averaged eastern tropical Pacific SAT (5 °S–5 °N, 150–90 °W)) in the GISS_new run accounts for ~30% of the amplitude of the observed Nino3 index (versus ~20% for the GISS_control run). The damped ENSO variability in both runs explains why the model cannot generate realistic polar–ENSO connectivities.

(2) The GISS_new run (Figure 5(b3)) also captures the observed meridional banding structure in the Atlantic (Figure 5(a3)) to some degree, whereas the GISS_control run does not (Figure 5(c3)).

(3) The GISS_new run (Figure 5(c3)) captures to some degree the observed tripole pattern extending from the South Pacific convergence zone through the Antarctic dipole region (Figure 5(a3)). By contrast, the GISS_control run only shows the dipole pattern in the Antarctic (Figure 5(b3)).

For each observed and model-based correlation map, significance tests that account for the temporal autocorrelations and spatial coherency in the datasets were conducted. Figure 6 shows the fraction of the entire global grid points in each correlation map with r-values exceeding the local 95% confidence level as functions of SIE band and lag intervals. This figure indicates which SIE bands are most likely sensitive to global teleconnections at various leads and lags. The SIE* regions showing the strongest and most persistent extrapolar links in the observations are the western Indian and eastern Pacific sectors of the Antarctic and the central Weddell Sea when SIE* lags SAT* from 0 to 2 years. The GISS_new run tends to reduce the erroneous strong circumpolar and broad Antarctic-wide coherency in the GISS_control run, as shown by the absence (presence) of the shading in the GISS_new (GISS_control) run in the central Pacific sector of the Antarctic (Figure 6). Although this improvement is somewhat encouraging, the GISS_new run misses the observed highly sensitive SIE regions in the eastern Pacific sector of the Antarctic.

To differentiate signal from noise in the correlation maps (showing the global distribution of correlation coefficients), we performed an EOF analysis on 270 correlation maps for the GISS_new run to detect the dominant and persistent teleconnection patterns between Antarctic SIE* and global SAT*. We then compared the EOF patterns with those arising from the correlation maps involving the observations and the GISS_control run. The first three modes of the observed correlation maps clearly display the main spatial patterns captured in the observed SAT* modes (cf. Figures 4 and 7). Both the GISS_control and GISS_new runs show the ENSO-like pattern and Antarctic dipole to some degree. The ENSO-like pattern and Antarctic dipole are in the third mode in the GISS_control run (Figure 7(b3)). They move up to the second mode and occupy more total variance in the GISS_new run, but with the wrong phase relationship between the tropics and southern high latitudes in the western hemisphere (Figure 7(c2)). In the first mode, the GISS_new run shows a signal in the western tropical Pacific that is not present in the GISS_control run. However, it has the wrong phase relationship with southern polar regions compared with the observations (Figure 7(c1)).

4. DISCUSSION AND CONCLUSIONS

This study seeks to determine whether the improved sea-ice and ocean processes in the GISS/CGCM capture observed Antarctic sea-ice variability and polar–extrapolar climate teleconnections better.

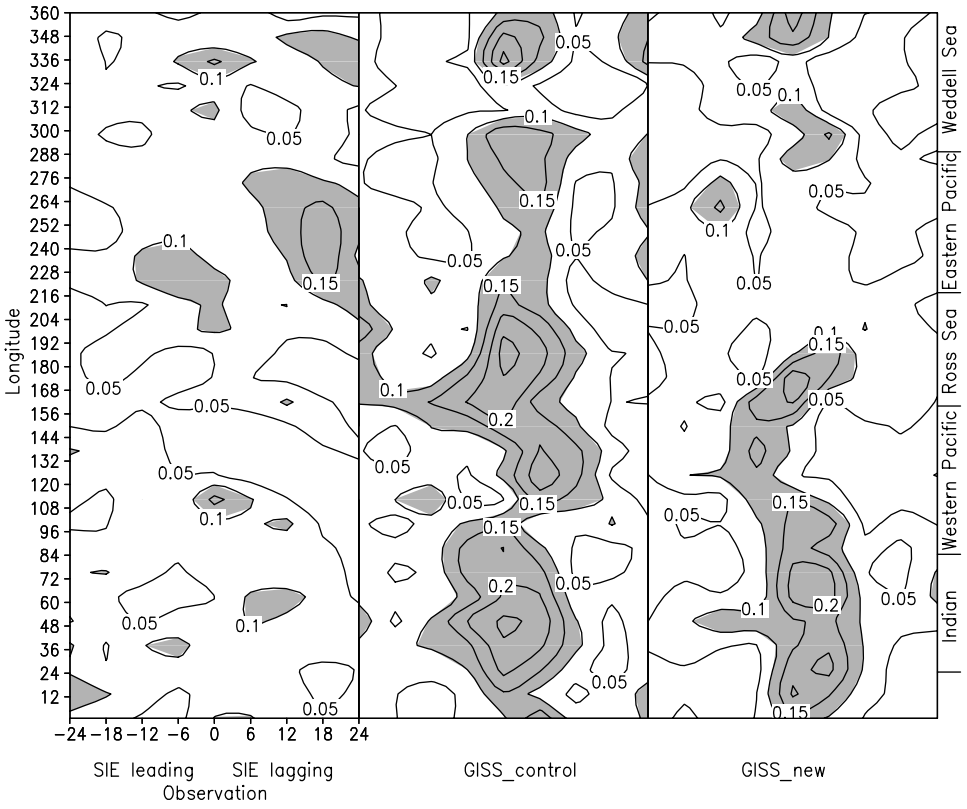

Figure 6. The fraction of total grid points in each correlation map that pass the local 95% significance test in the observation, GISS_control and GISS_new runs with SIE* leading 2 years to lagging 2 years (the fractions above 10% are shaded)

With the improvements in sea-ice dynamics and thermodynamics and in sub-grid-scale ocean processes, the GISS_new run does indeed do a better job in the representations of the local/regional ice–ocean interactions. For example, it improves the simulations of the seasonal distributions of the Antarctic sea-ice fields (edge and drift) and vertical temperature and salinity structure in the Southern Ocean in spring and winter, which are a consequence of improved sea-ice dynamics, sub-grid-scale ocean processes (particularly the Gent and McWilliam eddy isopycnal mixing with variable scaling mixing coefficients) and changes to ice–ocean boundary flux formulations (Liu *et al*., 2003a,b). The GISS_new run also slightly improves the simulated SAT climatology in the southern high latitudes.

Although the GISS_new run leads to some encouraging local/regional improvements as described above, these improvements do not extend to the simulations of the polar and extrapolar climate teleconnections. For example, there is no obvious change to the dominant spatial covarying patterns in SAT variability between the GISS_new and GISS_control runs at either the regional (southern high latitudes) or global scales. A small change is that the first SAT* EOF mode of the GISS_new run exhibits a signal in the western tropical Pacific that does not show up in the GISS_control run, but it has the wrong phase relationship with southern high latitudes (Figure 5). This pattern can also be found in the EOF analysis on the correlation maps (Figure 7). The simulated linkage between Antarctic SIE* and ENSO variability is still weak, and some dominant observed teleconnection patterns, such as the strong in-phase relationship between tropical South America and Africa, are still not well represented or are missed in the lead/lag correlation maps and EOF analysis on those correlation maps.

What are the possible causes of the weak teleconnections in the improved GISS/CGCM? (1) At the local/regional scale, although we have greatly improved sea-ice dynamics and thermodynamics and sub-grid ocean processes (which lead to improved local/regional ocean–ice interactions), we have not improved the

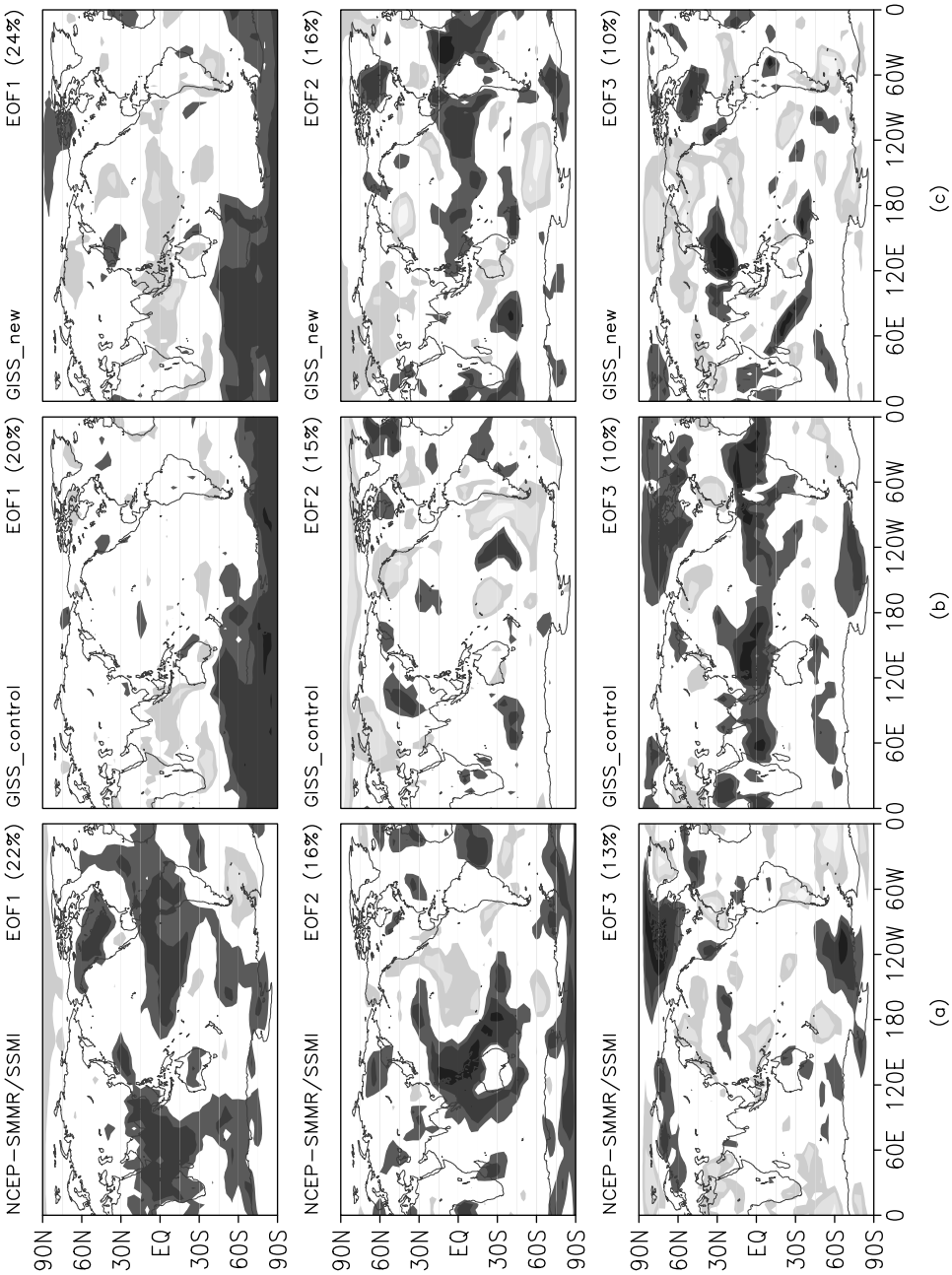

Figure 7. The first three leading EOF mode eigenvectors of the correlation fields generated by correlating 30 Antarctic SIE* bands and global SAT* of the observations (a) GISS_control (b) and GISS_new (c) at half-year intervals up to ±2 years

boundary interactions between the ice and the overlying atmosphere. Additional research, such as (a) coupling observed atmospheric forcings with the ice–ocean model and (b) driving the atmospheric model with observed sea-ice and ocean boundary conditions will elucidate whether the weak teleconnections are mainly due to continued shortcomings in the sea-ice model or the insufficient representations of the air–ice interactions within the boundary layer in the unaltered atmospheric model. (2) Weak teleconnections might also be caused by inadequate representations of some mid-latitude dynamic processes associated with the mean meridional atmospheric circulation and eddies in the model, which link the tropics and the high latitudes. A higher resolution model might be desired to do a better job in simulating these features, leading to proper polar–extrapolar climate covariability, which will be tested in the future work. (3) Finally, poor simulations of the tropical signals (the remote forcings to the polar regions) might be responsible for the weak teleconnections. For example, all the models in Liu *et al*. (2002), as well as in the GISS_new run, lack a dominant tropical ENSO mode, which would clarify and force proper response.

ACKNOWLEDGEMENTS

This research was supported by the NASA polar program and NOAA. The sea-ice concentration data were provided by the NOAA's National Snow and Ice Data Center.

REFERENCES

Carleton AM. 2003. Atmospheric teleconnections involving the Southern Ocean. *Journal of Geophysical Research* **108**: DOI: 10.1029/2000JC000379.

Curry JA, Webster PJ. 1999. *Thermodynamics of Atmospheres and Oceans*. Academic Press: London.

Ebert EE, Schramm JL, Curry JA. 1995. Disposition of shortwave radiation in sea ice. *Journal of Geophysical Research* **100**: 15 965–15 976.

Gent PR, McWilliams JC. 1990. Isopycnal mixing in ocean circulation models. *Journal of Geophysical Research* **20**: 150–155.

Gent PR, Willebrand J, McDougall TJ, McWilliams JC. 1995. Parameterizing eddy-induced tracer transports in ocean circulation models. *Journal of Physical Oceanography* **25**: 463–474.

Grenfell TC, Maykut GA. 1977. The optical properties of ice and snow in the Arctic basin. *Journal of Glaciology* **18**: 445–463.

Griffies S, Gnanadesikan MA, Pacanowski RC, Larichev V, Dukowicz JK, Smith RD. 1998. Isoneutral diffusion in a z-coordinate ocean model. *Journal of Physical Oceanography* **28**: 805–830.

Holland DM, Jenkins A. 1999. Modeling thermodynamic ice–ocean interactions at the base of an ice shelf. *Journal of Climate* **12**: 1787–1800.

Houghton JT, Ding Y, Griggs DJ, Noguer M, van der Linden PJ, Dai X (eds). *Climate Change 2001: The Scientific Basis*. Cambridge University Press: Cambridge, UK, 2001.

Liu J, Martinson DG, Yuan X, Rind D. 2002. Evaluating Antarctic sea ice variability and its teleconnections in global climate models. *International Journal of Climatology* **22**: 885–900.

Liu J, Schmidt GA, Martinson DG, Rind D, Russell G, Yuan X. 2003a. Sensitivity of sea ice to physical parameterizations in the GISS global climate model. *Journal of Geophysical Research* **108**(C2): DOI: 10.1029/2001JC001167.

Liu J, Schmidt GA, Martinson DG, Rind D, Russell G. 2003b. Improved treatments of sea ice thermodynamics in the GISS global climate model. *Journal of Geophysical Research* submitted for publication.

Levitus S, Boyer TP. 1994. *World Ocean Atlas 1994 Volume 4: Temperature*. NOAA Atlas NESDIS 4. US Department of Commerce: Washington, DC.

Levitus S, Burgett R, Boyer TP. 1994. *World Ocean Atlas 1994 Volume 3: Salinity*. NOAA Atlas NESDIS 3. US Department of Commerce: Washington, DC.

Martinson DG. 1990. Evolution of the Southern Ocean winter mixing layer and sea ice: open ocean deepwater formation and ventilation. *Journal of Geophysical Research* **95**: 11 641–11 654.

McPhee MG, Maykut GA. 1987. Dynamics and thermodynamics of the ice/upper ocean system in the marginal ice zone of the Greenland Sea. *Journal of Geophysical Research* **92**: 7017–7031.

Mitchell JF, Davis RA, Ingram WJ, Senior CA. 1995. On surface temperatures, greenhouse gases and aerosols: models and observations. *Journal of Climate* **8**: 2364–2386.

Rind D, Healy R, Parkinson C, Martinson DG. 1995. The role of sea ice in $2 \times CO_2$ climate model sensitivity. Part I: the total influence of sea ice thickness and extent. *Journal of Climate* **8**: 449–463.

Schramm JL, Holland MM, Curry JA. 1997. Modeling the thermodynamics of a sea ice thickness distribution, 1. Sensitivity to ice thickness resolution. *Journal of Geophysical Research* **102**: 23 079–23 091.

Visbeck M, Marshall J, Haine T, Spall M. 1997. On the specification of eddy transfer coefficients in coarse resolution ocean circulation models. *Journal of Physical Oceanography* **27**: 381–402.

Wajsowicz RC. 1993. A consistent formulation of the anisotropic stress tensor for use in models of the large-scale ocean circulation. *Journal of Computational Physics* **105**: 333–338.

Yuan X, Martinson DG. 2000. Antarctic sea ice variability and its global connectivity. *Journal of Climate* **13**: 1697–1717.

Zhang J, Hibler WD. 1997. On an efficient numerical method for modeling sea ice dynamics. *Journal of Geophysical Research* **102**: 8691–8702.

Zhang J, Rothrock D. 2000. Modeling Arctic sea ice with an efficient plastic solution. *Journal of Geophysical Research* **105**: 3325–3338.

